

# Template-free Sol-hydrothermal Synthesis of a Nitrogen Doped Anatase/Rutile/Brookite TiO<sub>2</sub> Nano-rod Bundle for Visible Light Driven Photocatalysis

Liu Zhengjiang<sup>1</sup>, Bao Xiaoli<sup>1</sup>, Xing Lei<sup>2</sup>, Yang Jucai<sup>1</sup>, Zhang Qiancheng<sup>1</sup>

<sup>1</sup> Key Laboratory of Industrial Catalysis of the Inner Mongolia Autonomous Region, Inner Mongolia University of Technology, Hohhot 010051, China; <sup>2</sup> Institute of Green Chemistry and Chemical Technology, Jiangsu University, Zhenjiang 212013, China

**Abstract:** Nitrogen doped anatase/rutile/brookite titanium dioxide (N-TiO<sub>2</sub>) regular nano-rod bundle photocatalyst for improving visible light photocatalytic activity was prepared through a template-free sol-hydrothermal method. The properties of the materials were characterized by X-ray diffraction (XRD), transmission electron microscopy (TEM), ultraviolet-visible diffuse reflectance spectra (UV-Vis DRS), Fourier transform infrared (FTIR) spectroscopy and X-ray photoelectron spectroscopy (XPS). Photocatalytic degradation of methyl orange (MO) in an aqueous solution under visible light irradiation was used as a probe reaction to evaluate the photocatalytic activity of the mixed-phase N-TiO<sub>2</sub> nano-rod bundle. The results of characterization combined with photocatalytic activity of MO photodegradation show that the synergistic effects among N doping, mixed-phase and nano-rod bundle structure are the main reasons to improve photocatalytic activity of mixed-phase N-TiO<sub>2</sub> nano-rod bundle compared with P25-TiO<sub>2</sub>. The possible mechanism of MO degradation by mixed phase N-TiO<sub>2</sub> nano-rod bundle photocatalyst was preliminarily discussed.

**Key words:** TiO<sub>2</sub> nano-rod bundle; mixed-phase tio<sub>2</sub>; nitrogen doping; visible light photocatalysis

Heterogeneous photocatalytic oxidation technology is an innovative method for the pollutant degradation. Titanium dioxide (TiO<sub>2</sub>) is typically used in photocatalysis reactions to try to achieve the total oxidation of organic and inorganic water pollutants. However, the large band gap energy restricts the practical application of TiO<sub>2</sub> because it can only utilize ultraviolet light<sup>[1-3]</sup>. Numerous efforts have been devoted to the photocatalytic efficiency improvement of TiO<sub>2</sub> in the visible-light range in the past few decades. It has been reported that doping anions into TiO<sub>2</sub> could result in the band gap narrowing to be more effective for enhancing the visible photocatalytic activity<sup>[4]</sup>. In these studies, nitrogen doping is regarded as one of the most important methods for potential application<sup>[5-9]</sup>. The light absorption onset of TiO<sub>2</sub> can be extended from the UV to the visible-light

range by nitrogen doping. The formation of an isolated narrow band above the valence band in TiO<sub>2-x</sub>N<sub>x</sub> or N 2p states contributes to the band gap narrowing by mixing with the 2p states of O<sup>[9]</sup>.

Recently, mixed-phase TiO<sub>2</sub> materials consisting of anatase, brookite and rutile have attracted widespread interest because the energy barrier among anatase, rutile and brookite suppresses electron transfer, which can inhibit the recombination of photoelectrons and holes to some extent<sup>[10]</sup>. Various methods have been reported for the synthesis of mixed-phase TiO<sub>2</sub> materials, such as sol-gel process, thermal oxidation and solvothermal synthesis<sup>[11]</sup>. However, among all these syntheses, morphology-controlled synthesis of complex nanostructure mixed-phase TiO<sub>2</sub> is still a great challenge<sup>[12]</sup>. It is desirable to develop a facile method to

Received date: January 09, 2018

Foundation item: National Natural Science Foundation of China (20966006); The Graduate Student Scientific Research Innovation Projects of the Inner Mongolia Autonomous Region (B20151012809)

Corresponding author: Zhang Qiancheng, Ph. D., Professor, School of Chemical Engineering, Inner Mongolia University of Technology, Hohhot 010051, P. R. China, Tel: 0086-471-6575722, E-mail: jzhang@imut.edu.cn

Copyright © 2019, Northwest Institute for Nonferrous Metal Research. Published by Science Press. All rights reserved.

design and synthesize complex nanostructure mixed-phase TiO<sub>2</sub> catalysts with excellent photocatalytic efficiency.

In this study, a template-free sol-hydrothermal method for the synthesis of nitrogen doped mixed-phase TiO<sub>2</sub> nano-rod bundle with regular morphology and visible light absorption was presented. The N species and the structure of N-TiO<sub>2</sub> nano-rod bundle were characterized by XRD, TEM, UV-Vis DRS, FTIR and XPS. The activity of the as-prepared nano-rod bundle was evaluated by the photocatalytic degradation of methyl orange (MO) under visible light irradiation.

## 1 Experiment

In a typical synthesis process, TiCl<sub>4</sub> (2.75 mL) was added dropwise in aqueous HCl solutions (50 mL, 2 mol/L) at room temperature with vigorous magnetic stirring of the reaction mixture in order to form the sol. Then, urea (4.5 g) was added into the sol with stirring. The resulting sol was transferred into a 100 mL Teflon-lined stainless steel autoclave and then heated to 120 °C for 18 h. Subsequently, the autoclave was allowed to cool naturally to room temperature. The obtained sample was filtered and washed with distilled water and dried at 100 °C in air. The nitrogen doped mixed-phase TiO<sub>2</sub> was labeled as N-TiO<sub>2</sub>.

X-ray diffraction (XRD) patterns were collected by a PANalytical Empyrean X-ray diffractometer with Cu K $\alpha$  radiation. The morphologies of the as-prepared N-TiO<sub>2</sub> were analyzed by transmission electron microscope (TEM) and high-resolution TEM (HRTEM) based on a FEI Tecnai F20 transmission electron microscope. X-ray photoelectron spectroscopy (XPS) was obtained by a PHI5000 Versa Probe X-ray photoelectron spectrometer with an Al K $\alpha$  (1486.6 eV) X-ray source. All binding energies were referred to the C 1s neutral carbon peak, which was assigned the value of 284.6 eV to compensate for surface charge effects. Fourier-transform infrared (FTIR) spectra of the samples were recorded by a Thermo Nicolet NEXUS FTIR spectrometer. Ultraviolet-visible diffuse reflectance spectra (UV-vis DRS) of the samples were obtained using an UV-3600PC spectrometer equipped with an integrating sphere.

MO photocatalytic degradations were performed to investigate the photocatalytic activity of N-TiO<sub>2</sub> nano-rod bundles under visible light irradiation. The photocatalytic activity of P25-TiO<sub>2</sub> was used for the comparison under the same conditions. A 300 W xenon lamp was used as the visible light source. Light with a wavelength below 420 nm was filtered by a cutoff filter. In a typical run, MO (250 mL, 20 mg/L) was mixed with the as-prepared N-TiO<sub>2</sub> photocatalyst (0.5 g) to prepare a suspension. The suspension was magnetically stirred for 90 min prior to irradiation to achieve adsorption-desorption equilibrium for MO. Then, the suspension was illuminated with the above-mentioned

light source. Part of suspension samples were taken from the reaction mixture every 30 min, followed by filtration through a 0.22  $\mu$ m PTFE syringe filter in order to remove the catalyst. The absorbance of the filtrate was then measured using the TU1901 UV-Vis spectrophotometer (Beijing, China). The MO concentration was obtained according to the linear relation between the absorbance at 464 nm and the concentration of MO. The degradation efficiency (%) was determined as  $(1 - C/C_0) \times 100\%$ , where  $C_0$  is the initial MO concentration and  $C$  is the MO concentration at different irradiation applications.

## 2 Results and Discussion

### 2.1 Microstructure of the as-prepared N-TiO<sub>2</sub>

The XRD pattern of the as-prepared N-TiO<sub>2</sub> is shown in Fig.1, which reveals that all three titania phases, namely, anatase, rutile and brookite simultaneously presented in the N-TiO<sub>2</sub>. According to the PDF cards in the XRD diffraction database, the peaks locating at  $2\theta = 48.05^\circ$ ,  $68.78^\circ$ ,  $70.01^\circ$  can be attributed to the diffractions of anatase from the (200), (116) and (220) planes (JCPDS No. 21-1272), respectively, while the peaks at  $2\theta$  of  $30.81^\circ$  and  $63.61^\circ$  are assigned to brookite (121) and (251) plane diffractions (JCPDS No. 29-1360). It is worth noting that the strong diffraction peak at  $2\theta$  of  $25.31^\circ$  of the anatase (101) plane can overlap with that of the brookite (120) plane. Therefore it needed to distinguish these two types of TiO<sub>2</sub> by comparing other diffraction peaks. In addition, the peaks at  $2\theta$  of  $27.35^\circ$ ,  $36.16^\circ$ ,  $41.23^\circ$ ,  $44.05^\circ$ ,  $54.33^\circ$  and  $56.69^\circ$  correspond to the diffractions of the (110), (101), (111), (210), (211) and (220) crystal planes of rutile phase TiO<sub>2</sub>, respectively (JCPDS No. 21-1276). XRD results confirm the coexistence of the brookite, anatase, and rutile in the N-TiO<sub>2</sub>. In many researches, it has been proved that the mixed-phase TiO<sub>2</sub> photocatalysts show a higher catalytic activity because of the effective separation of photo-excited charge carriers<sup>[13]</sup>.

The TEM and HRTEM micrographs of the as-prepared N-TiO<sub>2</sub> nano-rod bundles are displayed in Fig.2, which shows that numerous one-dimensional nano-rods were held

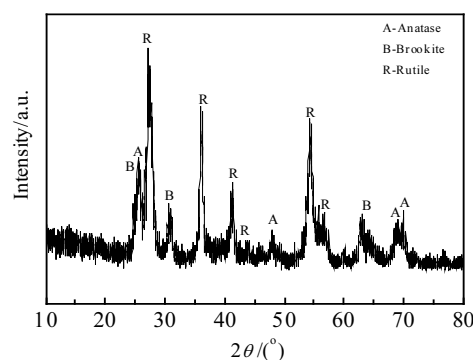


Fig.1 XRD pattern of the as-prepared N-TiO<sub>2</sub>

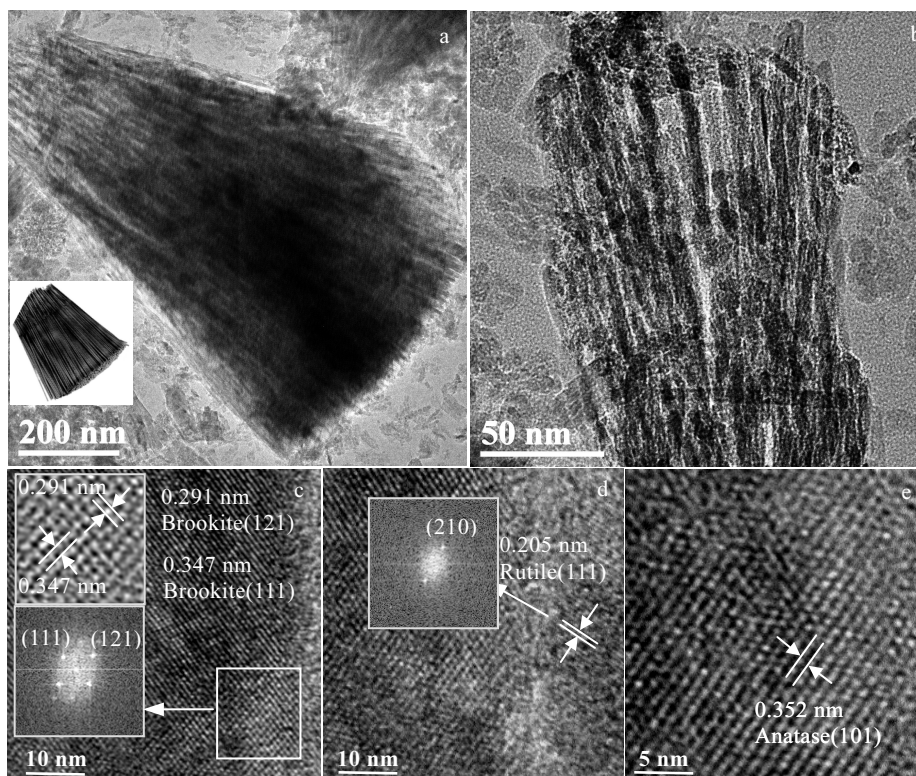


Fig.2 TEM (a, b) and HRTEM (c-e) micrographs of N-TiO<sub>2</sub> nano-rod bundle

together forming a straw bundle-like structure (i.e., nano-rod bundle). It is seen in Fig.2b that the nano-rod bundle has a hierarchical structure, which is very important in photocatalysis due to its distinctive physicochemical properties compared to conventional nanostructure crystallites such as slower electron-hole recombination rate, high light-harvesting capacity and more surface active sites<sup>[14]</sup>. Furthermore, the special morphology has a large number of interspaces among nano-rods which could offer potential pathways for the diffusion of charge carriers (photo-generated charge carriers), facilitating the redox process in the photocatalysis process<sup>[13]</sup>. As shown in Fig.2c, 2d and 2e, HRTEM was used to analyze the crystal properties of the N-TiO<sub>2</sub> nano-rod bundle. In Fig.2e, the nano-rod bundle shows an inter-planar spacing of 0.352 nm, corresponding to the (101) plane of anatase. However, the resolution of Fig. 2c and 2d was insufficient to provide atomic arrangement of the nano-rod bundle. Fast Fourier transform (FFT) and inverse FFT (IFFT) were therefore conducted to investigate the crystal structure of the as-prepared N-TiO<sub>2</sub> nano-rod bundle. After filtering out noise initiated by atomic defects and dislocation, the sharp patterns were obtained and converted to an image by inverting FFT (IFFT) as shown in Fig.2c. Inter-planar spacing of 0.291

nm were measured in the selected area, which can be assigned to the inter-planar distance of brookite (111) and (121), respectively. The FFT image (Fig. 2d) reveals the (210) planes of rutile TiO<sub>2</sub>. For rutile, the corresponding inter-planar spacing (210) is 0.205 nm. Results also indicate that the N-TiO<sub>2</sub> nano-rod bundle consists of brookite, anatase and rutile phases, being consistent with the three phases of nano-rods demonstrated by the XRD results.

## 2.2 Surface chemical analysis

The FTIR spectra of the N-TiO<sub>2</sub> and P25-TiO<sub>2</sub> samples are shown in Fig.3. The infrared absorption peak around 3425 cm<sup>-1</sup> is related to the stretching vibration of OH groups linked with titanium atoms (Ti-OH) and the peak around 1640 cm<sup>-1</sup> is the flexion vibration of OH group in adsorbed water. Compared to that of the P25-TiO<sub>2</sub>, the IR spectrum of N-TiO<sub>2</sub> shows more absorption peaks in the range of 1400–1550 cm<sup>-1</sup>. The peaks around 1450 and 1540 cm<sup>-1</sup> corresponding to N-H bond vibration indicate the presence of nitrogen in the synthesized sample<sup>[15]</sup>. The peak around 1400 cm<sup>-1</sup> can be assigned to the N-N stretching vibration<sup>[13]</sup>. It is noteworthy that the peaks around the 2334 and 2356 cm<sup>-1</sup> due to the formation of O-Ti-N linkage for N-doped TiO<sub>2</sub> are not observed<sup>[16]</sup>. This implies the presence of nitrogen doping into interstitial sites within the TiO<sub>2</sub> as opposed to the substitutional site within the lattice,

which was further verified by the XPS data.

Fig.4 shows the XPS spectra of the as-prepared N-TiO<sub>2</sub> nano-rod bundle. Through Gaussian fitting, as shown in Fig.4a, the N 1s peak can be separated into three peaks with binding energy (B.E.) of around 399.7, 401.4 and 406.0 eV. Peaks at 399.7 and 401.4 eV are indicative of the presence of nitrogen doping into interstitial sites<sup>[17]</sup>. It has been reported that the incorporation of interstitial nitrogen into the lattice of TiO<sub>2</sub> had beneficial effects on the visible light photocatalytic activity of TiO<sub>2</sub><sup>[18]</sup>. The peak around 406.0 eV was attributed to physisorbed N<sub>2</sub><sup>[19]</sup>. Fig.4b shows XPS spectrum of the O 1s of the N-TiO<sub>2</sub>. The O1s spectrum is resolved into two Gaussian curve-fitted peaks around 530.1 and 531.6 eV with B.E. The peak at 530.1 eV was assigned to the Ti–O bond (lattice O), and the highest B.E. peak was characteristic of titanium suboxide and/or adsorbed water<sup>[13]</sup>. Note that, the adsorbed water molecules are crucial for an efficient photocatalytic reaction, as they react with photo-excited holes to produce hydroxyl radicals (•OH) which in turn oxidize pollutant molecules in their vicinity. Fig.4c shows the fitted curve of Ti 2p XPS spectrum for the N-TiO<sub>2</sub>. It is clear that there are two major peaks located around 463.8 and 458.1 eV. The standard B.E. of Ti 2p<sub>1/2</sub> and 2p<sub>3/2</sub> in pure TiO<sub>2</sub> is

464.7 and 458.8 eV, respectively (NIST X-ray Photoelectron Spectroscopy Database). The B.E. of the Ti 2p<sub>3/2</sub> peak for N-TiO<sub>2</sub> has a shift of -0.7 eV in comparison to that of Ti 2p<sub>3/2</sub> in pure TiO<sub>2</sub>. The decrease in the B.E. of Ti 2p in N-doped TiO<sub>2</sub> indicates that TiO<sub>2</sub> lattice was modified to a considerable extent, due to N doping<sup>[20]</sup>. In brief, the peaks observed for N 1s, O 1s and the shift of Ti 2p peaks provided sufficient evidences for the interstitial incorporation of nitrogen in the TiO<sub>2</sub> lattice.

### 2.3 UV-vis DRS analysis

The UV-vis DRS of the as-prepared N-TiO<sub>2</sub> nano-rod bundle and P25-TiO<sub>2</sub> as a reference are shown in Fig. 5. Compared with the P25-TiO<sub>2</sub>, an obvious increase in the red shift of the absorption edge is observed for the N-TiO<sub>2</sub> nano-rod bundle sample. According to the relationship of the absorption edge  $\lambda_g$  (nm) and the band gap  $E_g$  (eV), the  $E_g$  was estimated as the following equation  $E_g = 1240/\lambda_g$ <sup>[21]</sup>. The red shift of the absorption edge indicates a decrease in the band gap. The original coordinates of the UV-vis spectrum registered for N-TiO<sub>2</sub> were transformed to Kubelka-Munk function (KM) versus photon energy ( $h\nu$ ) and then expressed as Tauc plot (inset of Fig.5), which show the relation of  $(KM \times h\nu)^{1/2} = f(h\nu)$ <sup>[22]</sup>. The value of the band gap was estimated as extrapolation of the linear part of the dependence. Thus, a 2.89 eV band gap of N-TiO<sub>2</sub> was obtained, which was less than that of brookite (3.0 eV), anatase (3.2 eV) and rutile (3.14 eV). The decreased band gap indicates an increased photo response range. In utilizing visible light, the as-prepared samples were thus capable of absorbing more photons, which could contribute to a more effective generation of electron-hole pairs<sup>[23]</sup>.

### 2.4 Visible light photocatalytic measurement

The visible light-induced photocatalytic activity of the as-prepared N-TiO<sub>2</sub> nano-rod bundle was evaluated through the photocatalytic degradation of the model pollutant, MO under visible light irradiation ( $\lambda \geq 420$  nm). The solution was stirred in the dark for 90 min before irra

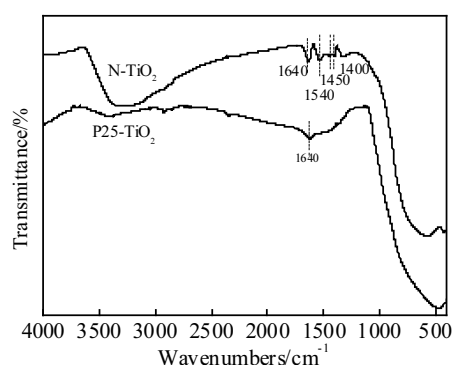


Fig.3 FTIR analysis of N-TiO<sub>2</sub> and P25-TiO<sub>2</sub>

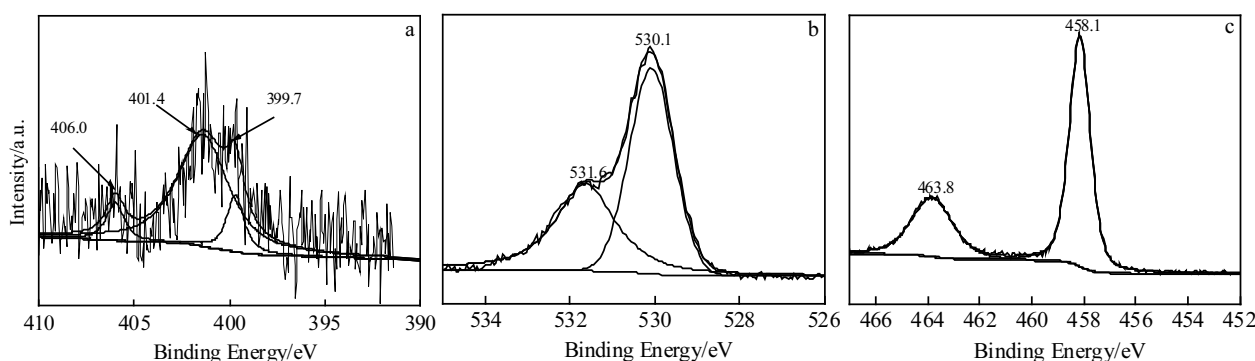
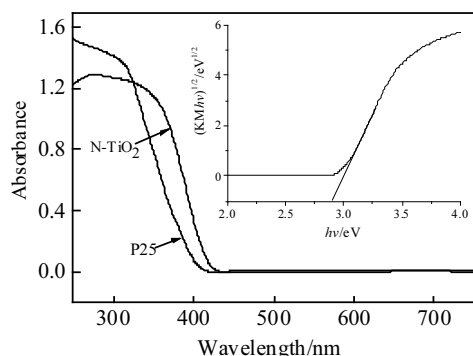
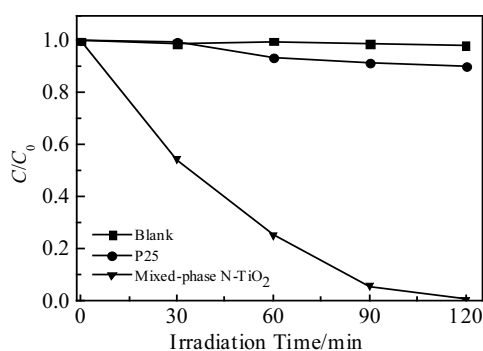
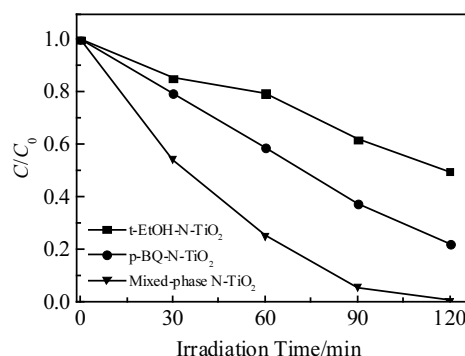


Fig.4 High-resolution XPS spectra for N 1s (a), O 1s (b) and Ti 2p (c) of N-TiO<sub>2</sub> nano-rod bundle

Fig.5 UV-vis DRS spectra of N-TiO<sub>2</sub> and P25-TiO<sub>2</sub>Fig.6 Visible photocatalytic degradations for MO solution using P25-TiO<sub>2</sub> and N-TiO<sub>2</sub> nano-rod bundle as catalysts

radiation to obtain equilibrium for MO. The change of the concentration of the unadsorbed MO was used to characterize the photocatalytic efficiency. Fig.6 shows the change in the relative concentrations of MO versus the visible light irradiation time. It is shown that N-TiO<sub>2</sub> nano-rod bundle exhibited much higher photocatalytic efficiency than P25-TiO<sub>2</sub> for the degradation of MO. When the irradiation time reached 120 min, the degradation efficiency of the blank, P25-TiO<sub>2</sub> and N-TiO<sub>2</sub> nano-rod bundle were approximately 2%, 12% and 98%, respectively. This improvement of photocatalytic performance of N-TiO<sub>2</sub> nano-rod bundle could be explained by the decreased recombination rate of the electrons and holes, which enhances the light-harvesting capacity and offers the potential pathways for the diffusion of photo-excited carriers in the N-TiO<sub>2</sub> nano-rod bundle photocatalyst.

To gain further insight into the reaction mechanism, active species quenching experiments using specific reagents including *t*-BuOH and *p*-BQ, were carried out to identify the contribution of  $\cdot\text{OH}$  and  $\text{O}_2^{\cdot-}$ . According to the literature, *t*-BuOH and *p*-BQ are very reactive toward  $\cdot\text{OH}$  and

Fig.7 Quenching experiments using *t*-BuOH and *p*-BQ in degrading MO in the N-TiO<sub>2</sub> nano-rod bundle system

$\text{O}_2^{\cdot-}$ , respectively<sup>[24, 25]</sup>. Fig.7 illustrates the influence of radical scavengers on the degradation of MO. It is clearly shown that in the absence of radical scavengers, MO was completely removed due to the generated oxidizing free radicals. Nevertheless, the addition of 20 mmol/L *t*-BuOH leads to a remarkably lower degradation of MO to 50% within 120 min, compared to the degradation profiles observed in the absence of scavengers. When *p*-BQ scavenger for  $\text{O}_2^{\cdot-}$  was added into the reaction system, the degradation of MO was also obviously affected, and the removal efficiency of MO decreases by 22% after adding 0.02 g *p*-BQ, which imply that  $\text{O}_2^{\cdot-}$  is also generated in the reaction process. Accordingly, the contribution of mainly  $\text{O}_2^{\cdot-}$  and  $\cdot\text{OH}$  to the MO degradation can be elucidated by comparing the difference in the process efficiency (in terms of MO degradation) between *t*-BuOH and *p*-BQ.

The effects of different parameters on the photocatalytic activity of N-TiO<sub>2</sub> nano-rod bundle are shown in Fig.8. The preparation conditions of the as-prepared N-TiO<sub>2</sub> photocatalyst were as follows: the sample preparation temperature from 120 °C to 180 °C and the sample preparation time from 6 to 24 h.

Fig.8a shows the visible light photocatalytic activities of the N-TiO<sub>2</sub> nano-rod bundles prepared at different preparation temperatures. It is found that for degradation of MO under visible light irradiation, the degradation efficiency decreased as the sol-hydrothermal temperature increased. Compared with the samples prepared at 140, 160 and 180 °C, the sample prepared at 120 °C showed the highest degradation efficiency and about 98% of MO was degraded after 120 min of visible light irradiation. On the other hand, the degradation efficiencies of all four samples were higher than 65%, indicating high photocatalytic activities of the samples prepared at temperatures above 120 °C.

Data for the N-TiO<sub>2</sub> nano-rod bundles prepared at different sol-hydrothermal time for the degradation of MO are

shown in Fig.8b. It was found that the sol-hydrothermal time significantly affected the degradation rate of MO under visible light irradiation, and the highest MO degradation efficiency was achieved at the sol-hydrothermal time of 18 h. This can be explained by the increase in the surface area, as shown in Fig.9. The sample prepared at 120 °C for 18 h showed the highest specific surface area ( $S_{\text{BET}}$ ) amongst the various sol-hydrothermal times of 6, 12, 18 and 24 h. The specific surface areas, as calculated using Brunauer-Emmet-Teller equation, are listed in Table 1. These values are in good consistence with the photocatalytic performance. According to the literature, higher specific surface areas and larger pore volumes of photocata-

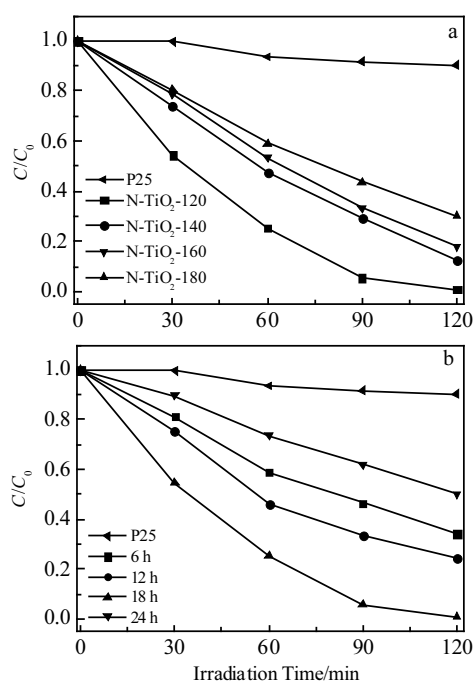


Fig.8 Photocatalytic degradation of MO using N-TiO<sub>2</sub> samples prepared by different conditions: (a) different reaction temperatures and (b) different reaction time

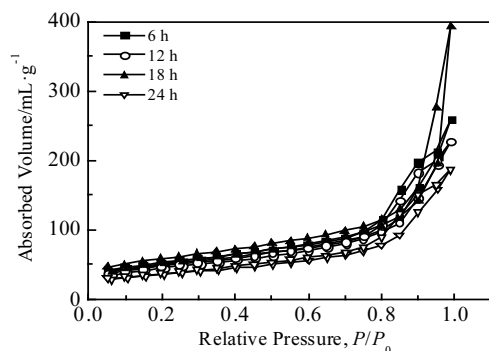


Fig.9 Nitrogen adsorption-desorption isotherms of N-TiO<sub>2</sub> samples prepared with different solvothermal time

**Table 1** Specific surface areas ( $S_{\text{BET}}$ ), pore diameters ( $D_p$ ) and pore volumes ( $V_p$ ) of different N-TiO<sub>2</sub> nano-rod bundles

Samples	N-TiO <sub>2</sub> (6 h)	N-TiO <sub>2</sub> (12 h)	N-TiO <sub>2</sub> (18 h)	N-TiO <sub>2</sub> (24 h)
$S_{\text{BET}}/\text{m}^2\cdot\text{g}^{-1}$	91.746	90.725	98.955	69.088
$D_p/\text{nm}$	3.091	3.063	3.061	3.845
$V_p/\text{mL}\cdot\text{g}^{-1}$	0.355	0.314	0.560	0.255

lysts both contributed to an enhanced photocatalytic activity owing to the presence of a large amount of surface active sites, so it can absorb and transfer reactant molecules easily via the interconnected porous structure, and increase the photocatalytic performance<sup>[26, 27]</sup>.

As discussed above, a preparation temperature of 120 °C and a preparation time of 18 h are found to be the optimum conditions for the mixed phase N-TiO<sub>2</sub> nano-rod bundles for the highest photocatalytic activities.

## 2.5 Synergistic effects of N doping, mixed-phase and nano-rod bundle structure

The N-TiO<sub>2</sub> nano-rod bundle shows a higher photocatalytic activity than P25-TiO<sub>2</sub> under visible light irradiation (Fig. 6). N doping into TiO<sub>2</sub> interstitial sites is discussed above, according to the XPS result. N incorporation at the interstitial structure could introduce a new N 2p energy level situated above the valence band compared to pristine TiO<sub>2</sub> and narrow band gap that promoted the acceleration of photogenerated electrons from TiO<sub>2</sub><sup>[16]</sup>. Thus, it facilitated the availability of photogenerated holes to interact with the chemisorbed water and/or hydroxyl group of producing hydroxyl radical ( $\cdot\text{OH}$ ). At the same time, electrons could subsequently reduce the surface adsorbed oxygen ( $\text{O}_2$ ) to oxygen radicals ( $\text{O}_2\cdot^-$ ) radicals. These hydroxyl radicals and oxygen radicals have very strong oxidizing ability that helps the as-prepared samples to attract and degrade the MO molecule in the aqueous media. Meanwhile, brookite, anatase and rutile phases were detected in XRD and HRTEM analysis. When anatase, brookite and rutile are in contact with each other, once they are excited by light, the electrons will be excited from the valence band into the conduction band, and then different band structure at the interface allows the charge transfer (i.e., transfer of electrons) from one phase to another<sup>[28,29]</sup>, which effectively separates the charges with the electrons accumulating in one phase and the holes in another, and thereby the photogenerated electron/hole pairs could be efficiently separated among the three phases. The synergistic effect would increase the photocatalytic activity of N-TiO<sub>2</sub> nano-rod bundle to a certain degree. In addition, nano-rod bundle structure was also detected by TEM. It has been reported that nanorods or nanowires could suppress the charge recombination and improve the charge transport<sup>[30]</sup>.

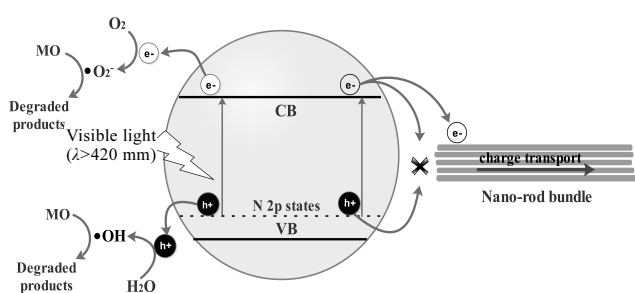


Fig.10 Schematic illustrations for the synergistic effect of photocatalytic degradation of MO on the N-TiO<sub>2</sub> nano-rod bundle in visible light

Moreover, according to the literature, interfacial structure of nano-rod in the TiO<sub>2</sub> polymorphs would include large amounts of tetrahedral Ti<sup>4+</sup> sites, which could serve as hot spots for photocatalytic activity and thus make the mixed-phase nanocrystals into an effective photocatalytic relay for visible light utilization<sup>[31]</sup>. These factors resulted in an enhanced photocatalytic efficiency of mixed phase N-TiO<sub>2</sub> nano-rod bundle photocatalysts under visible light irradiation. A schematic illustration of photocatalytic degradation for MO on the surface of N-TiO<sub>2</sub> nano-rod bundle photocatalysts is shown in Fig.10.

### 3 Conclusions

1) Anatase/rutile/brookite N-TiO<sub>2</sub> nano-rod bundle photocatalysts are successfully synthesized through a facile and low-cost sol-hydrothermal method, which is template-free synthesis.

2) N-TiO<sub>2</sub> nano-rod bundle with visible photocatalytic activity can effectively catalyze MO degradation in an aqueous solution. The improved photocatalytic performance of N-TiO<sub>2</sub> nano-rod bundle is ascribed to the synergistic effects of N doping, mixed phases and the nano-rod bundle. N doping makes the TiO<sub>2</sub> band gap narrower, resulting in an improvement in the photocatalytic response to visible light.

3) Brookite, anatase and rutile are generated on N-TiO<sub>2</sub> nano-rod bundle, which improve the photocatalytic activity of N-TiO<sub>2</sub> nano-rod bundle by separating the photo-generated electron/hole pairs.

4) Nano-rod bundle offers potential pathways for the diffusion of charge carriers (photo-generated charge carriers), facilitating the redox process during the photocatalysis process.

### References

- 1 Lu K, Liang Y, Li W. *Materials Letters* [J], 2012, 89(24): 77
- 2 Radoičić M B, Janković I A, Despotović V N et al. *Applied Catalysis B: Environmental*[J], 2013, 138-139(14): 122

- 3 Zhang Chunyong, Li Mingshi, Lu Mohong et al. *Rare Metal Materials and Engineering*[J], 2017, 46(2): 0322 (in Chinese)
- 4 Xu H, Ouyang S, Liu L et al. *Journal of Materials Chemistry A* [J], 2014, 2(32): 12642
- 5 Valentin C D, Finazzi E, Pacchioni G et al. *Chemical Physics*[J], 2007, 339 (1-3): 44
- 6 Gupta S M, Tripathi M. *Chinese Science Bulletin*[J], 2011, 56(16): 1639
- 7 Pan L, Zou J J, Wang S et al. *Applied Surface Science*[J], 2013, 268(3): 252
- 8 Diwald O, Thompson T L, Zubkov T et al. *The Journal of Physical Chemistry B*[J], 2004, 108: 6004
- 9 Nolan N T, Synnott D W, Seery M K et al. *Journal of Hazardous Materials*[J], 2012, 211-212(2): 88
- 10 Liao Y, Que W, Jia Q et al. *Journal of Materials Chemistry*[J], 2012, 22(16): 7937
- 11 Jung K Y, Park S B, Jang H D. *Catalysis Communications*[J], 2004, 5(9): 491
- 12 Li H, Shen X, Liu Y et al. *Journal of Alloys and Compounds*[J], 2015, 646: 380
- 13 Gai L, Duan X, Jiang H et al. *Cryst Eng Comm*[J], 2012, 14: 7662
- 14 Tian G, Chen Y, Zhou W et al. *Cryst Eng Comm*[J], 2011, 13(8): 2994
- 15 Gomathi Devi L, Eraiah Rajashekhar K. *Journal of Sol-Gel Science and Technology*[J], 2011, 60(2): 144
- 16 Bakar S A, Byzinski G, Ribeiro C. *Journal of Alloys and Compounds*[J], 2016, 666(5): 38
- 17 Mohamed M A, Salleh W N W, Jaafar J et al. *Materials Chemistry and Physics*[J], 2015, 162(15): 113
- 18 Dunnill C W H, Aiken Z A, Pratten J et al. *Journal of Photochemistry & Photobiology A Chemistry*[J], 2009, 207(2-3): 244
- 19 Wadhwa S, Mathur A, Hamilton J W J et al. *Advanced Science, Engineering and Medicine*[J], 2015, 7: 1
- 20 Xu X, Song W. *Materials Technology*[J], 2017, 32(1): 52
- 21 Zhang Q, Shan A, Wang D et al. *Journal of Sol-Gel Science and Technology*[J], 2013, 65(2): 204
- 22 Mamulova Kutlakova K, Tokarsky J, Kovar P et al. *Journal of Hazardous Materials*[J], 2011, 188(1-3): 212
- 23 Zhang L, Tse M S, Tan O K et al. *Journal of Materials Chemistry A*[J], 2013, 1(14): 4497
- 24 Yang M Q, Zhang Y, Zhang N et al. *Scientific Reports*[J], 2013, 3: 3314
- 25 Michael-Kordatou I, Iacovou M, Frontistis Z et al. *Water Research*[J], 2015, 85: 346
- 26 Hao R, Wang G, Tang H et al. *Applied Catalysis B: Environmental*[J], 2016, 187: 47
- 27 Dong G, Ho W, Li Y et al. *Applied Catalysis B: Environmental* [J], 2015, 174-175: 477
- 28 Xu H, Zhang L. *Journal of Physical Chemistry C*[J], 2009, 113(5): 1785
- 29 Zachariah A, Baiju K V, Shukla S et al. *Journal of Physical*

- 30 Yang N, Zhai J, Wang D et al. *ACS Nano*[J], 2010, 4(2): 887
- 31 Li G, Dimitrijevic N M, Chen L et al. *Journal of the American Chemical Society*[J], 2008, 130(16): 5402

## 无模板剂的溶胶-水热法合成具有可见光响应的氮掺杂 混晶 TiO<sub>2</sub> (锐钛矿/金红石/板钛矿) 纳米棒束

刘正江<sup>1</sup>, 鲍晓丽<sup>1</sup>, 邢磊<sup>2</sup>, 杨桔材<sup>1</sup>, 张前程<sup>1</sup>

(1. 内蒙古工业大学 内蒙古自治区工业催化重点实验室, 内蒙古 呼和浩特 010051)

(2. 江苏大学 绿色化学与化工技术研究院, 江苏 镇江 212013)

**摘要:** 采用无模板剂的溶胶-水热法制备了具有可见光响应的 N 掺杂锐钛矿/金红石/板钛矿型 TiO<sub>2</sub>(N-TiO<sub>2</sub>) 纳米棒束, 并利用 X 射线衍射(XRD)、透射电镜(TEM)、紫外-可见光漫反射光谱(UV-Vis DRS)、傅里叶变换红外光谱(FTIR)和 X 射线光电子能谱(XPS)等手段对获得的样品进行了表征。以甲基橙为模型反应物, 评价了 N-TiO<sub>2</sub> 纳米棒束的光催化活性。表征结果结合光催化活性评价结果显示, 与 P25-TiO<sub>2</sub> 相比, N 掺杂、混晶及纳米棒束之间的协同作用是所制备的混晶 N-TiO<sub>2</sub> 纳米棒束具有良好光催化活性的主要原因, 并对混晶 N-TiO<sub>2</sub> 纳米棒束光催化降解甲基橙的机理进行了探讨。

**关键词:** TiO<sub>2</sub> 纳米棒束; 混晶 TiO<sub>2</sub>; 氮掺杂; 可见光光催化

---

作者简介: 刘正江, 男, 1988 年生, 博士生, 内蒙古工业大学化工学院, 内蒙古 呼和浩特 010051, 电话: 0471-6575722, E-mail: zhengliu@126.com